Journal of Water Process Engineering 59 (2024) 105022

Contents lists available at ScienceDirect

Journal of Water Process Engineering

journal homepage: www.elsevier.com/locate/jwpe

Modeling complete and shortcut simultaneous nitrification and denitrification coupled to phosphorus removal in moving bed biofilm reactors

Anna Lanzetta [a,*], Davide Mattioli [b], Francesco Di Capua [c], Vincenzo Minieri [a], Stefano Papirio [a], Giovanni Esposito [a]

[a] Department of Civil, Architectural and Environmental Engineering, University of Naples Federico II, Via Claudio 21, 80125 Naples, Italy
[b] Laboratory Technologies for the Efficient Use and Management of Water and Wastewater, Italian National Agency for New Technologies, Energy and Sustainable Economic Development (ENEA), Via M.M. Sole 4, 40129 Bologna, Italy
[c] School of Engineering, University of Basilicata, via dell'Ateneo Lucano 10, 85100 Potenza, Italy

ARTICLE INFO

Editor: Ludovic F. Dumée

Keywords:
Mathematical modeling
Model calibration
and validation
Wastewater treatment
Moving bed biofilm reactor
Simultaneous nitrification denitrification
Phosphorus removal

ABSTRACT

This study aimed to model simultaneous nitrification and denitrification (SND) and shortcut (partial) SND processes coupled to phosphorus removal in lab-scale moving bed biofilm reactors based on data collected during two different experimental campaigns. Modeling was performed using BioWin 6.0 to accurately predict the experimental results. A sensitivity analysis conducted for the first experimental campaign identified the most influential process parameters. The absolute variance, Thiel's inequality coefficient, and normal objective function were used to evaluate the consistency of the experimental and modeled data. The calibrated and validated models satisfactorily reproduced the experimental data for all experimental campaigns and within the acceptance criteria, resulting in a suitable tool for predicting the process efficiency. Moreover, calibrated and validated data were used to test different dissolved oxygen (DO) ranges (0.6–0.8 mg $O_2 \cdot L^{-1}$), pH (6.5–9.0), and hydraulic retention time (HRT) (0.5–1.0 d) to improve shortcut SND. Based on the different simulated scenarios, the intermittent DO conditions can induce and maintain the inhibition of the nitrite-oxidizing bacteria with an average N-NO_3^- concentration of 0.05 mg $N \cdot L^{-1}$, while an HRT of 0.9 d resulted in average effluent N-NH_4^+, N-NO_3^- and N-NO_2^- concentrations of 4.0, 0.02 and 0.07 mg $\cdot L^{-1}$, respectively, indicating an efficient shortcut SND process.

1. Introduction

The removal of nitrogen (N) and phosphorus (P) from wastewater is of crucial importance in controlling the eutrophication process, which is responsible for the excessive growth of algae and, consequently, a depletion of dissolved oxygen (DO) in the receiving water bodies [1–4]. Conventionally, biological N removal (BNR) in wastewater treatment plants (WWTPs) includes autotrophic nitrification and heterotrophic denitrification implemented in sequence according to different possible configurations [5]. During nitrification, ammonium is oxidized to nitrate by ammonia-oxidizing bacteria (AOB) and nitrite-oxidizing bacteria (NOB) under aerobic conditions. Heterotrophic denitrification consists of nitrate (NO_3^-) reduction to dinitrogen gas (N_2) under anoxic conditions with organic carbon as the electron donor [6]. However, this approach results in energy-intensive aeration [7], high capital and operating costs, a large footprint, and high sludge production [8].

Phosphorus removal primarily relies on methods such as adsorption, chemical precipitation, or biological processes [7–9,11]. Compared to the other P removal systems, enhanced biological phosphorus removal (EPBR) with activated sludge systems is a cost-effective and environmentally sustainable alternative to chemical treatment [10,14]. The EBPR process achieves P removal by cycling anaerobic-aerobic metabolisms of phosphate-accumulating organisms (PAO) [14].

Simultaneous nitrification and denitrification (SND) is considered a promising alternative to conventional nitrification and denitrification processes for N removal within a single bioreactor, as it offers several advantages mainly associated with a lower footprint, carbon demand, sludge production, and oxygen requirement [15]. Moreover, no recirculation of nitrified effluent is needed, which simplifies the process

* Corresponding author.
E-mail address: anna.lanzetta@unina.it (A. Lanzetta).

https://doi.org/10.1016/j.jwpe.2024.105022
Received 24 November 2023; Received in revised form 22 January 2024; Accepted 16 February 2024
Available online 22 February 2024

Nomenclature

μ_{AOB}	maximum specific growth rate AOB [d^{-1}]
$b_{AOB,aerobic}$	aerobic decay rate AOB [d^{-1}]
$b_{AOB,anoxic/anaerobic}$	anoxic/anaerobic decay rate AOB [d^{-1}]
$K_{SB,AOB}$	substrate half saturation AOB [mg N·L^{-1}]
$K_{O2,AOB}$	ammonia oxidizing DO half saturation [mg O_2·L^{-1}]
μ_{NOB}	maximum specific growth rate NOB [d^{-1}]
$b_{NOB,aerobic}$	aerobic decay rate NOB [d^{-1}]
$b_{NOB,anoxic/anaerobic}$	anoxic/anaerobic decay rate AOB [d^{-1}]
$K_{SB,NOB}$	substrate half saturation NOB [mg N·L^{-1}]
$K_{O2,NOB}$	nitrite-oxidizing biomass DO half saturation [mg O_2·L^{-1}]
μ_H	maximum specific growth rate OHO [d^{-1}]
Y_H	heterotrophic biomass yield [mg COD·mg COD^{-1}]
$b_{H,aerobic}$	aerobic decay rate OHO [d^{-1}]
$b_{H,anoxic}$	anoxic decay rate OHO [d^{-1}]
$K_{SB,OHO}$	substrate half saturation OHO [mg COD·L^{-1}]
μ_{PAO}	maximum specific growth rate PAO [d^{-1}]
Y_{PAO}	PAO biomass yield [mg COD·mg COD^{-1}]
$b_{PAO,anaerobic}$	anaerobic decay rate PAO [d^{-1}]
$b_{PAO,anoxic/aerobic}$	anoxic/aerobic decay rate PAO [d^{-1}]
$K_{SB,PAO}$	substrate half saturation PAO [mg COD_{PHB}·mg COD_{PAO}^{-1}]
$K_{O2,PAO}$	phosphorus accumulating DO half saturation [mg O_2·L^{-1}]
$K_{P\ uptake}$	phosphate uptake half saturation constant [mg P·L^{-1}]
Diff. N-NH_4^+	biofilm diffusivity of N-NH_4^+ [m^2 d^{-1}]
Diff. N-NO_3^-	biofilm diffusivity of N-NO_3^- [m^2 d^{-1}]
Diff. N-NO_2^-	biofilm diffusivity of N-NO_2^- [m^2 d^{-1}]
Diff. oxygen	biofilm diffusivity of oxygen [m^2 d^{-1}]
Diff. acetate	biofilm diffusivity of acetate [m^2 d^{-1}]
Diff. acetate	biofilm diffusivity of acetate [m^2 d^{-1}]
Diff. neta	80 % of the specified effective diffusivities [−]
FZno	fraction of total influent COD which is nitrite-oxidizing organisms [g COD·g COD^{-1}]
L1	Film surface area to media area ratio – max [μm]

scheme and reduces the energy requirement. One of the main factors affecting the successful occurrence of SND is the oxygen diffusion limitation, which leads to the formation of an anoxic microenvironment in the inner parts of sludge flocs or adhered biofilms and allows the coexistence of autotrophic nitrifying and heterotrophic denitrifying microorganisms at different layers of the same stratified structure [16].

Recent studies showed that the SND process can be coupled to successful phosphorus removal [10,17].

According to Zaman et al. [17], the simultaneous nitrification, denitrification, and phosphorus removal (SNDPR) process requires less organic matter and DO consumption than the conventional biological phosphorus removal. Recent research has also focused on the shortcut (or partial) SND pathway involving partial nitrification or *nitritation* (NH_4^+ oxidation to NO_2^-) and *denitritation* (NO_2^- reduction to N_2) instead of complete nitrification and denitrification pathways. By eliminating the NO_2^- oxidation (*nitratation*) step, the shortcut pathway is advantageous compared to the complete pathway as less organic carbon and oxygen are needed for BNR. However, suppression of NOB activity is needed, which can be pursued via several strategies, including strict control of DO, pH, solid retention time (SRT), temperature, and concentrations of free ammonia and nitrous acid [15].

To date, various bioreactor configurations have been tested for SND processes, including the sequential batch reactor (SBR) [18,19], membrane bioreactor (MBR) [20], moving bed biofilm reactor (MBBR) [12–14], and aerobic granular sludge (AGS) reactor [15,16,24]. Compared with suspended-growth systems, biofilm-based technologies have shown several advantages, including higher biomass concentration, lower space requirements, shorter retention time, reduced sludge production, and more stable performances [26].

The growing interest in biofilm-based treatment processes has been accompanied by an increasing focus on their numerical analysis and biofilm modeling studies. Mathematical modeling is an important tool to predict the performance of a biological treatment, determine important variables and critical parameters, and aid in troubleshooting [27]. Additionally, the use of simulations during modeling can improve the WWTP design by providing different bioreactor operation scenarios [28]. Many biofilm models are incorporated in most of the currently used simulation software, such as Simba# (Ifak GmbH, Magdeburg, Germany), AQUASIM® (EAWAG, Switzerland), BioWin (Envirosim Associates Ltd.), and WEST (MIKE DHI®) [29]. The dynamic mixed-culture biofilm model implemented in BioWin belongs to the class of 1D models, as described by Wanner and Reichert [30,31]. In summary, the mathematical model of mixed-culture biofilms consists of a series of 1D mass balance equations that allow to model the progression of biofilm thickness as well as the spatial distribution and development over time of various dissolved (nutrients, electron donors, and electron acceptors) and particulate components (microbial cells, extracellular polymeric substances, organic and inorganic particles) in a biofilm as a function of transport and transformation processes [30,32].

Compared to the previous multispecies biofilm models [33], the dynamic mixed-culture biofilm model of BioWin permits a more flexible description of the transport of dissolved components in the biofilm and considers the diffusive transport of particulate components in the biofilm solid matrix, changes in the biofilm liquid phase volume fraction (porosity), and simultaneous detachment and attachment of cells and particles at the biofilm surface [30]. The process model integrated with the biofilm model in BioWin is the activated sludge/anaerobic digestion model (ASDM), which allows to simulate the complex interactions occurring in the aerobic, anoxic, and anaerobic layers of the biofilm. Despite the growing interest in SND processes and the empirical mathematical models supporting their successful implementation, calibrated models using experimental data are scarce in the literature [25,26,34]. Specifically, none of the abovementioned studies include the modeling of the complete and shortcut SNDPR processes.

The present study contributes to filling the existing gap in this field by modeling complete and shortcut SNDPR in MBBRs based on the data collected from two different experimental campaigns conducted at a laboratory scale by Iannacone et al. [22,23]. The main objective of this work is to assess whether a calibrated and validated model could accurately predict the experimental results. By using the BioWin software, different operating conditions, including dissolved oxygen (DO), feed carbon-to-nitrogen (C/N) ratio, and hydraulic retention time (HRT), were simulated with the aim of investigating the main impacts on the process in terms of removal of the main wastewater contaminants (i.e., COD, ammonium, oxidized nitrogen species and phosphate) and evolution of the dominant functional groups (i.e., AOB, NOB, ordinary heterotrophic organisms (OHO), and PAO). Additionally, the validated model from the second experimental campaign was used to test alternative scenarios to improve nutrient removal efficiencies, thus representing an important aid for potential future successful implementation and scale-up of the process.

2. Materials and methods

2.1. Experimental data

The experimental data from two different campaigns [22,23] were used to calibrate and validate the biofilm model implemented in BioWin 6.0. Specifically, the studies were based on long-term (shortcut) SNDPR in continuous-flow MBBRs under different operational conditions,

involving changes in C/N, HRT, and DO concentration, as reported in Table S1.

The MBBRs were fed exclusively with synthetic wastewater containing acetate, NH_4^+, and PO_4^{3-} as the main sources of organic carbon, nitrogen, and phosphorus, respectively. DO, pH, and HRT were monitored as reported by Iannacone et al. [22,23].

The first experimental campaign lasted 137 days and was divided into 6 experimental periods (P1-P6). The continuous-flow MBBR (intermittent-aeration MBBR, IAMBBR) was operated under alternating microaerobic and aerobic conditions with the aim of removing carbon, nitrogen, and phosphorus through SNDPR [22]. The HRT was set to 1 day and different DO conditions and C/N ratios were tested. The values of the input parameters used in BioWin for the simulations are reported in Tables S2. The input flow rate was constant for the entire calibration and validation periods and equal to 0.02 $m^3 \cdot d^{-1}$ in accordance with the HRT value of 1 day. The fractionation of total COD (tCOD), TKN, total phosphorous (TP), and total sulfur (TS) used in the BioWin model are reported in Table S3. In particular, the fraction of acetate was set to the maximum value allowed of 0.97 to simulate the presence of only readily biodegradable organic matter in the influent. The temperature was set at 22 °C according to the experimental campaign, while to reproduce the DO profiles of the microaerobic-aerobic cycles applied during the experimental campaign [22] an oxygen time trend based on the experimental DO profiles was considered for the simulations (Table S4). For the first two experimental periods (P1 and P2), as detailed experimental data were not available, the DO concentration trend used for the simulation was reproduced considering the experimental DO ranges, while for P3-P6 a cyclic variation in oxygen over time was reconstructed based on the experimental DO profiles.

The second experimental campaign lasted 125 days and investigated the feasibility of coupling shortcut SND with biological P removal in two continuous-flow IAMBBRs alternating microaerobic and aerobic conditions and fed with two different carbon sources, i.e., ethanol and acetate [23].

The reactors were operated at an HRT of 1 day, DO ranges of 0.2–3.0 mg $O_2 \cdot L^{-1}$, and feed C/N ratios between 3.6 and 4.0 in both reactors (Table S1) [13]. NOB activity was inhibited by cultivating the biomass at a temperature of 26–28 °C, a pH of 8.2 ± 0.2, and an SRT of 4 days before MBBR inoculation. The input dataset used in BioWin for the simulations is reported in Table S5. The input flow rate was constant for the entire calibration and validation periods in accordance with the calibration of the first experimental campaign. The temperature value set in the model was higher than the temperature during the first experimental campaign and equal to 30 °C (on average), according to the temperature measured during the experiment (in the range of 26–32 °C). To reproduce the experimental aeration conditions [23], a time trend of the DO based on the experimental data was considered during the dynamic simulations (Table S6). In the absence of experimental data, BioWin's default values were used to set the initial values, and a steady-state simulation was performed. This simulation generated the initial values of the main active biomasses used in the dynamic simulation of both experimental campaigns.

2.2. Biofilm model calibration

Model calibration can be described as an iterative process to reproduce the observed values by adjusting input model parameters. The calibration procedure followed in this study was based on six main stages as proposed by Rieger [36], including 1) the identification of different calibration and validation datasets, 2) refinement of the stop criteria based on data quality and availability, 3) initial run of the model using default kinetics and stoichiometric parameter values on BioWin, 4) sensitivity analysis to obtain the reproduction of the biofilm models and optimize the efficiency of the calibration procedure, 5) calibration, and 6) validation.

The sensitivity analysis allows to check the sensitivity of the output variables to varying parameters, inputs, or initial conditions. The sensitivity analysis of the biofilm parameters was carried out using the normalized sensitivity coefficient ($S_{i,j}$), which is a ratio between the output variable (Y_i) and the input variable (X_i) (Eq. 1), as reported by Eldyasti et al. [29].

$$S_{i,j} = \left| \frac{\Delta Y_i / Y_i}{\Delta X_i / X_i} \right| \quad (1)$$

The influence of the parameters was interpreted as proposed by Julien et al. [37]. If $S_{i,j}$ is equal to zero, the parameters have no influence. For $S_{i,j} < 0.25$, the influence of the parameter is not considered to be significant. If $0.25 < S_{i,j} < 1$, the parameter is influential. If $S_{i,j} > 1$, the parameters are very influential. The sensitivity analysis was carried out only for the first experimental campaign by increasing the selected parameter values by 5 % compared to the default values and recording the effect on several output variables. Only the most influential parameters were considered for the calibration procedure. The analysis comprised 21 kinetic parameters of AOB, NOB, OHO, and PAO biomass, 5 diffusion coefficients, and 4 biofilm parameters.

The model calibration of the first experimental campaign was carried out using the monitoring data collected from periods P1 to P4 (Table S1). For the second experimental campaign, the model calibration was also performed using the monitoring data collected from periods P1 to P4 (Table S1) starting with the calibrated model from the previous experimental campaign. During the cultivation phase of the second experimental campaign, NOB growth in the MBBR was successfully inhibited by setting specific SRT, pH, and temperature conditions, as described in Section 2.1. To simulate the same conditions in the model, the μ_{NOB} and FZno parameters were set to 0 during a preliminary steady-state step.

To compare the measured and simulated data in the calibration and validation procedure, the absolute variance S_{ai} was chosen as the acceptance criterion (Eq. 2):

$$S_{ai} = |\overline{y_s} - \overline{y_m}| \quad (2)$$

where y_s is the average simulated data and y_m is the average measured data.

For each experimental campaign, the absolute variance S_{ai} must be lower than 5 % of y_m. A maximum S_{ai} value ($S_{ai,max}$) of 2.5 mg $N \cdot L^{-1}$ was considered acceptable for $N\text{-}NH_4^+$, $N\text{-}NO_3^-$, and $N\text{-}NO_2^-$ concentrations. For COD and total P concentrations, maximum values of 20 mg $COD \cdot L^{-1}$ and 1.0 mg $P \cdot L^{-1}$ were considered. Furthermore, Thiel's inequality coefficient (*TIC*), as suggested by Hvala [38], (Eq. 3), and the normal objective function (*NOF*), as shown in Eq. 4 [27], were chosen as additional acceptance criteria.

$$TIC = \frac{\sqrt{\sum_i (y_i - y_{m,i})^2}}{\sqrt{\sum_i y_i^2} + \sqrt{\sum_i y_{m,i}^2}} \quad (3)$$

$$NOF = \sqrt{\frac{\sum_i (y_i - y_{m,i})^2}{N}} \frac{N}{\sum_i y_i} \quad (4)$$

y_i represents the measured data points, $y_{m,i}$ represents the computed data points, and N is the number of data points [39].

TIC values should be between 0 and 1, with values closer to 0 indicating a better model validity [27]. Zeng et al. [39] suggested that the values of *TIC* that do not exceed 0.3 are usually considered evidence of good agreement between the time series. Moreover, *NOF* values <1 reveal good reproducibility between the experimental and modeled data.

Table 1
Calibration of the parameters of the dynamic models of the two experimental campaigns.

	Unit	Experimental campaign	Experimental campaign	BioWin	Literature range	Reference
		I	II	Default		
Detachment rate	d^{-1}	4000	4000	8000	–	This study
Y_H	mg COD·mg COD^{-1}	0.540	0.540	0.666	0.21–0.90	[27,40]
Y_{PAO}	mg COD·mg COD^{-1}	0.520	0.520	0.639	0.625–0.821	[53]
$b_{H,anoxic}$	d^{-1}	0.62	0.62	0.233	0.2–0.6	[22,33], [35,38]
$K_{SB,\ OHO}$	mg COD·L^{-1}	5	5	5	5–20	[55]
$K_{O2,OHO}$	mg O_2·L^{-1}	0.15	0.15	0.15	0.05–0.20	[15,17], [39]
Anoxic growth factor, $_{OHO}$	–	0.2	0.2	0.5	–	This study
$b_{PAO,anoxic/anaerob}$	d^{-1}	0.20	0.10	0.10	0.15–0.20	[31,41]
$K_{P\ uptake}$	mg P·L^{-1}	0.50	0.20	0.15	–	This study
$K_{O2,\ PAO}$	mg O_2·L^{-1}	0.025	0.025	0.05	–	This study
$K_{SB,AOB}$	mg N·L^{-1}	1.20	1.20	0.7	1	[57]
μ_{AOB}		0.7	0.9	0.9	0.77–1	[27,31]
$K_{O2,\ AOB}$	mg O_2·L^{-1}	1.09	1.3	0.25	0.2–0.75	[36]
$K_{SB,NOB}$	mg N·L^{-1}	1.0	0.7	0.1	–	This study
$K_{O2,NOB}$	mg O_2·L^{-1}	0.89	1.10	0.5	0.2–0.75	[27,31]

3. Results and discussion

3.1. Modeling complete and shortcut SND in continuous-flow IAMBBR

3.1.1. Sensitivity analysis

The significant results of the sensitivity analysis for the soluble COD, N-NH_4^+, N-NO_3^-, N-NO_2^-, and P-PO_4^{3-} concentrations, as well as for biomass thickness, are reported in Fig. S1.

The sensitivity analysis showed that the significant factors for COD and N-NH_4^+ abatement were linked to the growth of the heterotrophic and autotrophic biomass (i.e., μ_H and μ_{AOB}), respectively (Fig. S1). The N-NO_3^- concentration was influenced by the kinetic parameters of NOB (i.e., $b_{NOB,aerobic}$ and $b_{NOB,anoxic/anaerobic}$), OHO ($b_{H,anoxic}$), PAO (μ_{PAO}), and mainly by oxygen diffusivity in the biofilm, which can be ascribed to high sensitivity of denitrifiers to oxygen. Typically, the presence of oxygen has a detrimental effect on denitrifying activity through enzyme inhibition or alteration of their gene expression [40]. The NO_2^- concentration was mainly sensitive to changes in the kinetic parameters of NOB ($b_{aerobic,\ NOB}$, $b_{anaerobic,\ NOB}$, μ_{NOB}, $K_{SB,NOB}$) and oxygen diffusivity in the biofilm. For typical BNR, the NO_2^- generated from NH_4^+ oxidation is subsequently oxidized to NO_3^- by NOB under aerobic conditions [41]. Therefore, a DO limitation could lead to NOB inhibition and a subsequent increase in NO_2^- concentration. For P-PO_4^{3-} concentration, the most significant variations were related to the change of the kinetic parameters of OHO ($b_{H,aerobic}$, μ_H, $K_{SB,OHO}$) and PAO ($b_{PAO,anoxic/aerobic}$) due to substrate competition between PAO and denitrifiers [42]. Furthermore, changing the attachment and detachment rates significantly affected the biofilm thickness. Precisely, particulate attachment and detachment rates have a major role in establishing biofilm thickness, dynamics, and biomass activity in the system [32]. Biofilm development is determined by a combination of physical and physiological processes, including attachment, cell growth, endogenous decay, and detachment [43]. The particulate attachment rate in BioWin is related to the bulk particulate concentration, while the detachment rate is a combined function reflecting the most important variables affecting film detachment, such as film thickness, extracellular polymerase substances (EPS) strength coefficient, and the effect of N_2 or CH_4 gas generation inside the deeper film layers. Fig. S2 shows the sensitivity analysis conducted on the average biomass concentrations of the main microbial functional groups present in the bioreactor, including AOB, NOB, OHO, and PAO. The results of the sensitivity analysis confirmed that attachment and detachment rates had a significant impact on the growth of microorganisms. Specifically, an increased detachment rate results in a higher concentration of the active biomass in the biofilm. This can be explained by the fact that in systems with a high detachment (or shear) force, the biofilm becomes more compact, with less filamentous structure growth [44]. This results in an increase in biomass in the biofilm.

3.1.2. Model calibration

Table 1 shows the kinetic, stoichiometric, and biofilm parameters used in the dynamic model calibration for the two experimental campaigns compared with their default values in BioWin and literature values. According to Eldyasti et al. [29] and Boltz et al. [45], three sequential calibration changes should be followed in biofilm processes to fit the experimental data: (1) the biofilm thickness (by setting the appropriate values of the attachment and/or detachment rates), (2) the biomass stoichiometry parameters, and finally (3) the kinetics. In biofilm models, the biofilm thickness is predominantly governed by the detachment rate. Therefore, the first step was to calibrate the biofilm thickness by gradually reducing the detachment rate up to 50 % compared to its default value. According to the model results, as the detachment rate decreases, the biofilm thickness tends to increase. The reduction was made not to exceed a biofilm thickness of 1.5 mm, a value consistent with experimental observations [22,23]. After the adjustment of biofilm thickness, in accordance with the calibration procedure [29], the default values of stoichiometric coefficients of OHO and PAO, i.e., Y_H and Y_{PAO}, were calibrated and reduced from 0.666 to 0.540 and 0.639 to 0.520 mg COD·mg COD^{-1}, respectively. Other studies on experimental biofilms [46] have reported even lower yields than those used in this study. In a previous study, Eldyasti et al. [29] observed a Y_H value of 0.36 mg COD•mg COD^{-1} in fluidized bed respirometers. In another study aimed at modeling the process of partial nitrification and denitrification in a hybrid biofilm reactor, a Y_H value of 0.52 mg COD•mg COD^{-1} was found. Furthermore, for the application of biofilm mathematical models, Trojanowicz et al. [47] recommend Y_H values ranging from 0.206 to 0.900 mg COD•mg COD^{-1}.

Regarding the calibration of kinetic parameters, it was necessary to intervene on the heterotrophs by reducing the anoxic growth factor of OHO, which in the model represents the fraction of microorganisms capable of growing under anoxic conditions, and/or by reducing the growth rate under anoxic conditions, while at the same time increasing the default value of $b_{H,anoxic}$. These modifications are consistent with the consideration that the high SRTs of attached growing systems are compatible with higher decay rates compared to the activated sludge process. Specifically, the anoxic factor of OHO biomass and $b_{H,anoxic}$ were set at 0.2 and 0.62 d^{-1}, respectively. Other changes involved a reduction in PAO growth kinetics. To better match the experimental and calibrated results of the first experimental campaign, the decay coefficient $b_{PAO,Anoxic/aerob}$ was increased from 0.1 to 0.2 d^{-1} according to Henze [48]. These changes were made considering that in the absence of a specific anaerobic phase, typical PAO does not develop in the reactor. Indeed, microbial community analyses performed on the carrier-attached biomass collected from the experimental reactor showed high

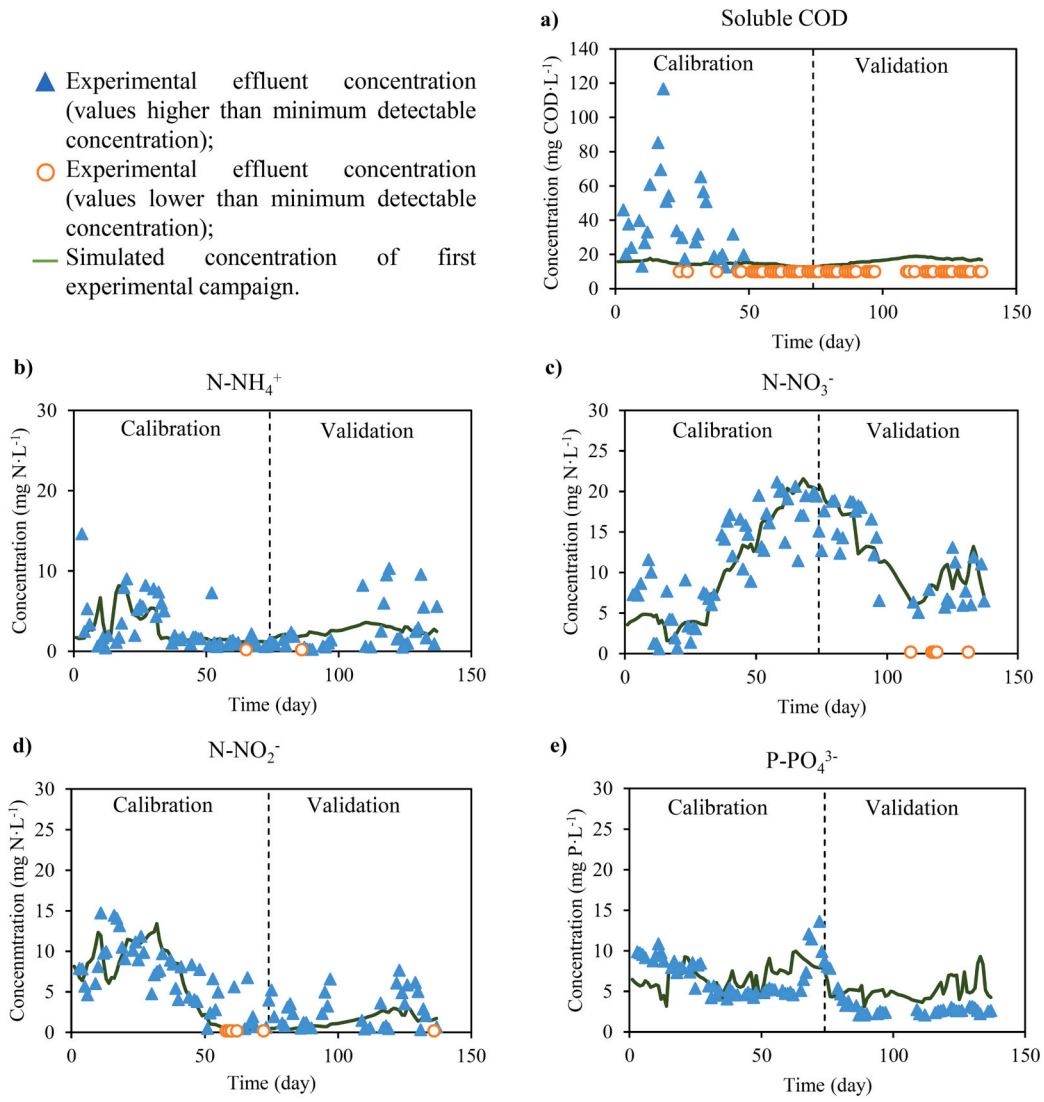

Fig. 1. Comparison of measured and simulated effluent concentrations of soluble COD, N-NH_4^+, N-NO_3^-, N-NO_2^- and P-PO_4^{3-} obtained during the first experimental campaign. The minimum detectable concentrations were equal to 10 mg·L^{-1} for COD and 0.2 mg·L^{-1} for N-NH_4^+, N-NO_3^-, N-NO_2^-, and P-PO_4^{3-}.

Table 2
Absolute variance S_{ai}, Thiel's inequality coefficient (*TIC*), and the normal objective function (*NOF*) used as acceptance criteria in the calibration and validation processes of the first experimental campaign.

Calibration model			
	S_{ai} [mg·L^{-1}]	*TIC*	*NOF*
Soluble COD	9.5	–	–
N-NH_4^+	0.2	0.42	1.10
N-NO_3^-	1	0.14	0.32
N-NO_2^-	0.4	0.23	0.55
P-PO_4^{3-}	0.0	0.19	0.40

Validation model			
	S_{ai} [mg·L^{-1}]	*TIC*	*NOF*
Soluble COD	–	–	–
N-NH_4^+	0.0	0.43	1.10
N-NO_3^-	1	0.19	0.44
N-NO_2^-	1.2	0.50	0.95
P-PO_4^{3-}	1.8	0.33	0.92

S_{ai} = average value in the calibration and validation periods.

relative abundances of atypical P-accumulating denitrifiers (e.g. Hydrogenophaga) [22] characterized by accumulation rates lower than those of typical PAO bacteria [49]. Hence, $K_{Puptake}$ was increased from 0.15 to 0.50 mg P·L^{-1} in the first and to 0.20 mg P·L^{-1} in the second experimental campaign. This parameter stops the growth of PAO biomass with polyphosphate storage at low soluble P concentration, thus impacting the concentration of soluble effluent P. In addition, to accurately reproduce experimentally measured N removals at low concentrations, other parameters that were acted upon are $K_{O2,\ AOB}$ and $K_{O2,\ NOB}$, which were increased from 0.25 to 1.09 and 0.89 mg O_2·L^{-1} in the first experimental campaign and from 0.5 to 1.3 and 1.1 mg O_2·L^{-1} in second experimental campaign in order to limit NH_4^+ and NO_2^- oxidation respectively by AOB and NOB at low DO conditions [32]. The difference in calibration between the two experimental campaigns is acceptable due to the different biomass cultivation methods and operational conditions.

3.1.3. Model validation

After calibration, the model of the first experimental campaign was validated using data from different periods (P5-P6) than those used for calibration (P1-P4) (Table S1). Fig. 1 shows the simulations performed on both the calibration and validation periods. Table 2 reports the absolute variance S_{ai} as well as the TIC and NOF indicators used for the

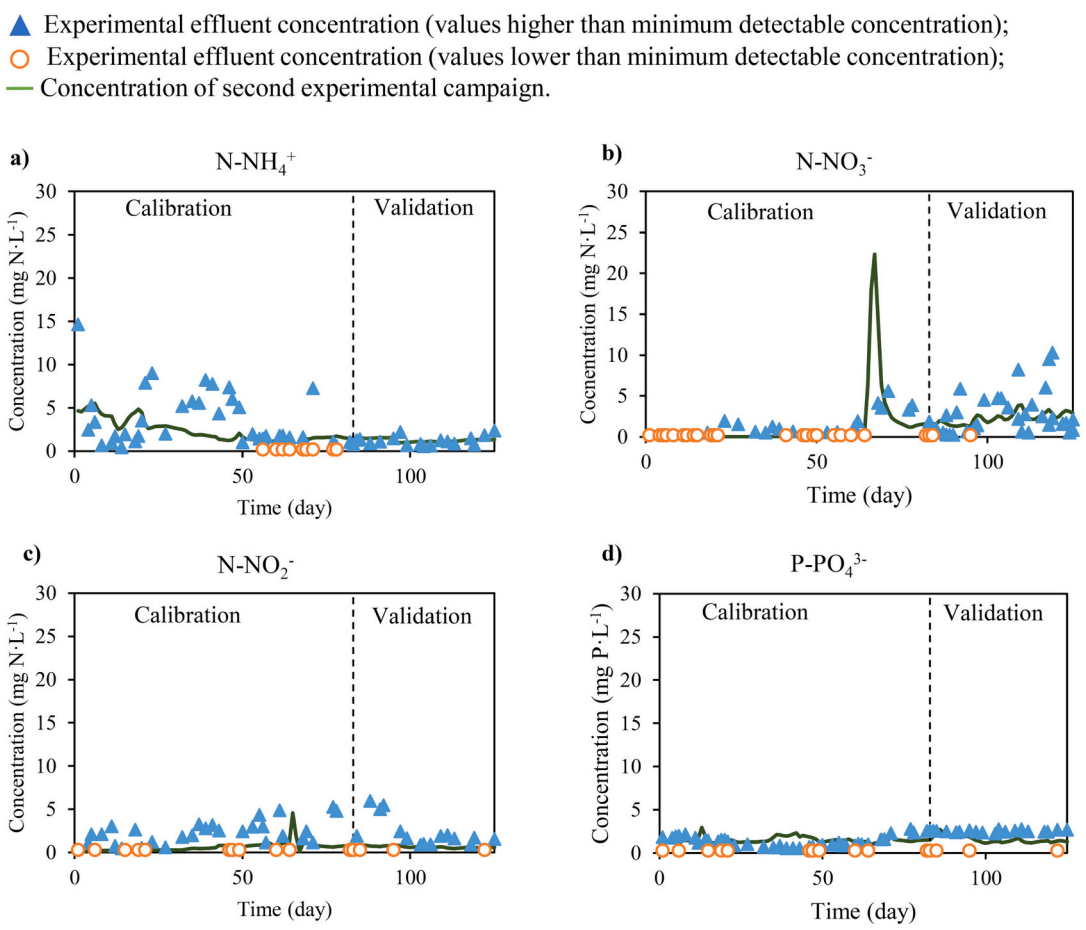

Fig. 2. Comparison of measured and simulated concentrations in terms of $N\text{-}NH_4^+$, $N\text{-}NO_3^-$, $N\text{-}NO_2^-$, and $P\text{-}PO_4^{3-}$ for the second experimental campaign. The minimum detection values for the ion concentrations were equal to 0.2 $mg{\cdot}L^{-1}$.

calibration and validation of the model. The indicators show a good correspondence between experimental and modeled values, and the soluble COD, $N\text{-}NH_4^+$, $N\text{-}NO_3^-$, $N\text{-}NO_2^-$, and $P\text{-}PO_4^{3-}$ concentrations showed a similar trend compared to the experimental data (Fig. 1, Table 2). The higher discrepancy observed in the fit of the data was related to the concentration of soluble COD in P1. Specifically, for the soluble COD, it was not possible to evaluate the concentrations because all measured data were below the analytical detection limit (<10 mg $COD{\cdot}L^{-1}$). For $N\text{-}NH_4^+$ and $N\text{-}NO_2^-$ concentrations, the obtained TIC and NOF values during calibration and validation can be accepted due to the low effluent NH_4^+ and NO_2^- concentrations. It should be noted that the acceptance indicators refer to the relative difference. Therefore, a small absolute variation could produce a significant relative deviation if values are low. The other acceptance indicators are perfectly within the literature ranges. Consequently, the results obtained for all analyzed parameters showed a good simulation of data by the calibrated model.

The validation procedure of the second experimental campaign was also carried out using a different dataset (P5-P6) instead of calibration periods (P1-P4) (Table S1). Fig. 2 shows the results obtained from the calibration and validation steps. The measured COD values were lower than the detection values, thus it was not possible to compare them to the simulated data. The calibrated model showed a good reproduction of the measured data for all analyzed parameters (Fig. 2). The peak in the plot of the $N\text{-}NO_3^-$ concentration was caused by a sudden change in aeration patterns from microaerobic to aerobic conditions with the aim of reproducing the reactor operating conditions (Fig. 2b). Indeed, due to a malfunctioning of the DO control system, on day 69 an increase in DO concentration to approximately 5 $mg{\cdot}L^{-1}$ was observed and lasted for two days, resulting in an unexpected growth of NOB biomass [23]. For these days only, the DO concentration in the model was set to the fixed value of 5 $mg{\cdot}L^{-1}$ to reproduce the experimental conditions.

Table 3
Absolute variance S_{ai}, Thiel's inequality coefficient (*TIC*), and the normal objective function (*NOF*) used as acceptance criteria in the calibration and validation processes of the second experimental campaign. The measured COD values could not be compared with the simulated data due to the COD value being lower than the detection value.

Calibration model			
	S_{ai} [mg L^{-1}]	*TIC*	*NOF*
$N\text{-}NH_4^+$	0.0	0.38	0.98
$N\text{-}NO_3^-$	0.2	0.46	2.33
$N\text{-}NO_2^-$	1.1	0.64	1.12
$P\text{-}PO_4^{3-}$	0.1	0.25	0.56

Validation model			
	S_{ai} [mg L^{-1}]	*TIC*	*NOF*
$N\text{-}NH_4^+$	0.8	0.48	0.95
$N\text{-}NO_3^-$	0.3	0.33	0.69
$N\text{-}NO_2^-$	1.3	0.66	1.10
$P\text{-}PO_4^{3-}$	0.9	0.25	0.40

S_{ai} = average value in the calibration and validation periods.

Table 3 shows the results of S_{ai}, TIC, and NOF used as acceptance criteria in the calibration and validation processes of the second experimental campaign.

For the $N\text{-}NH_4^+$ and $N\text{-}NO_2^-$ concentrations, even if TIC and NOF are

Table 4
Modeled scenarios for the shortcut SND process with different aeration patterns, pH, and HRT.

Scenario	Proposed actions
1	1.0 Intermittent aeration without DO failure (0.2–3.0 mg $O_2 \cdot L^{-1}$)
	1.1 DO range equal to P4 period of second campaign (0.2–2.0 mg $O_2 \cdot L^{-1}$)
	1.2 DO concentration = 0.8 mg $O_2 \cdot L^{-1}$
	1.3 DO concentration = 0.6 mg $O_2 \cdot L^{-1}$
2	2.1 pH value = 8.1 (starting condition)
	2.2 pH value = 6.5
	2.3 pH value = 8.4
	2.4 pH value = 9.0
3	3.1 HRT value = 1.0 d
	3.2 HRT value = 0.9 d
	3.3 HRT value = 0.75 d
	3.4 HRT value = 0.5 d

higher than the acceptance threshold, the calibrated model can be accepted due to the low absolute variance values. For the N-NO_3^- and P-PO_4^{3-} concentrations, the TIC and NOF indicators are perfectly within the literature ranges, thus indicating the goodness of fit of the calibrated and validated mathematical model.

3.2. Evolution of microbial functional groups in the biofilm

The trends of the biomass composing the microbial biofilm within the MBBRs for the two modeled campaigns are shown in Fig. S3. Biomass trends for the first campaign (Fig. S3a) showed a slight growth of AOB biomass, except in P6. The trend of NOB biomass was quite steady, with a gradual increase during P4 due to the higher value of DO (Table S1). As expected, the trend in OHO and PAO biomass was dependent on the change in COD concentration. During P2-P5, there was a slight decrease in the concentrations of OHO and PAO biomass due to the lower COD levels in the system, while an increase in OHO and PAO biomass was observed during P6 in accordance with the higher COD concentrations in the experimental data [22].

The simulated trends of AOB and NOB biomass during the second campaign are shown in Fig. S3b. The NOB and AOB biomass trends agree with the experimental results. From day 65, due to the increase in DO concentration in the reactor, the NOB biomass increased. Instead, the AOB biomass remained constant in all experimental periods.

3.3. Model optimization of the shortcut SND process

The experimental results of the second campaign confirmed the advantages of the shortcut SND process over complete SND in terms of removal efficiency for the various contaminants. For this reason, the validated model of this campaign was used to test alternative scenarios to improve N removal while ensuring successful NOB inhibition. The modeled scenarios involved changes in the aeration conditions, pH, and HRT, as shown in Table 4. First, the shortcut SND in the MBBR was modeled without considering the DO control malfunctioning during days 65–67 in order to assess the potential of intermittent aeration conditions to inhibit NOB growth effectively.

Fig. 3 illustrates the results in terms of N-NH_4^+, N-NO_3^-, AOB, and NOB biomass under intermittent aeration conditions. The results confirm that intermittent aeration can effectively induce and maintain NOB inhibition. Comparing the experimental and simulated data (intermittent aeration without failure), no significant difference can be

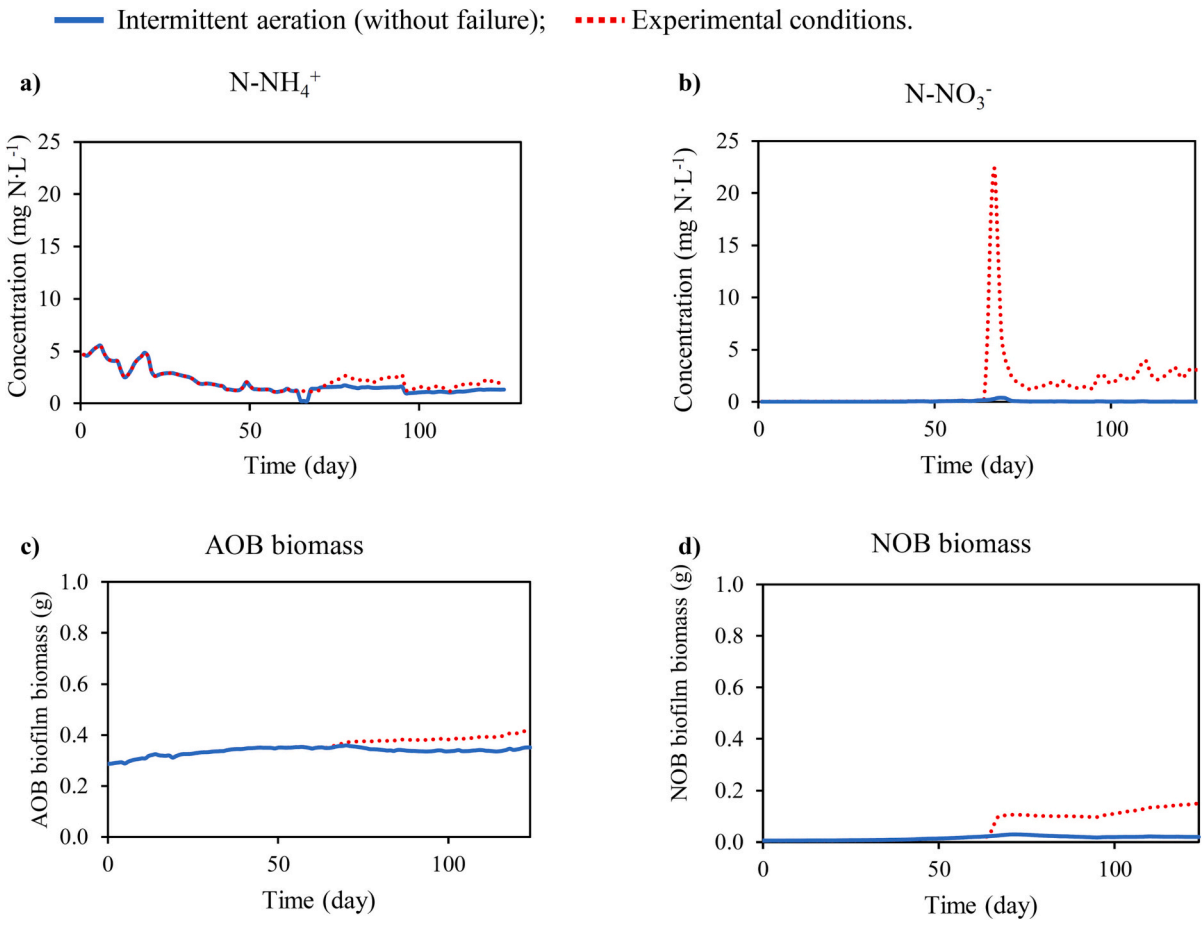

Fig. 3. Comparison of simulated effluent nitrogen (N-NH_4^+, N-NO_3^-) and biomass (AOB, NOB) concentration trends under experimental and modeled (without DO system failure) intermittent aeration conditions.

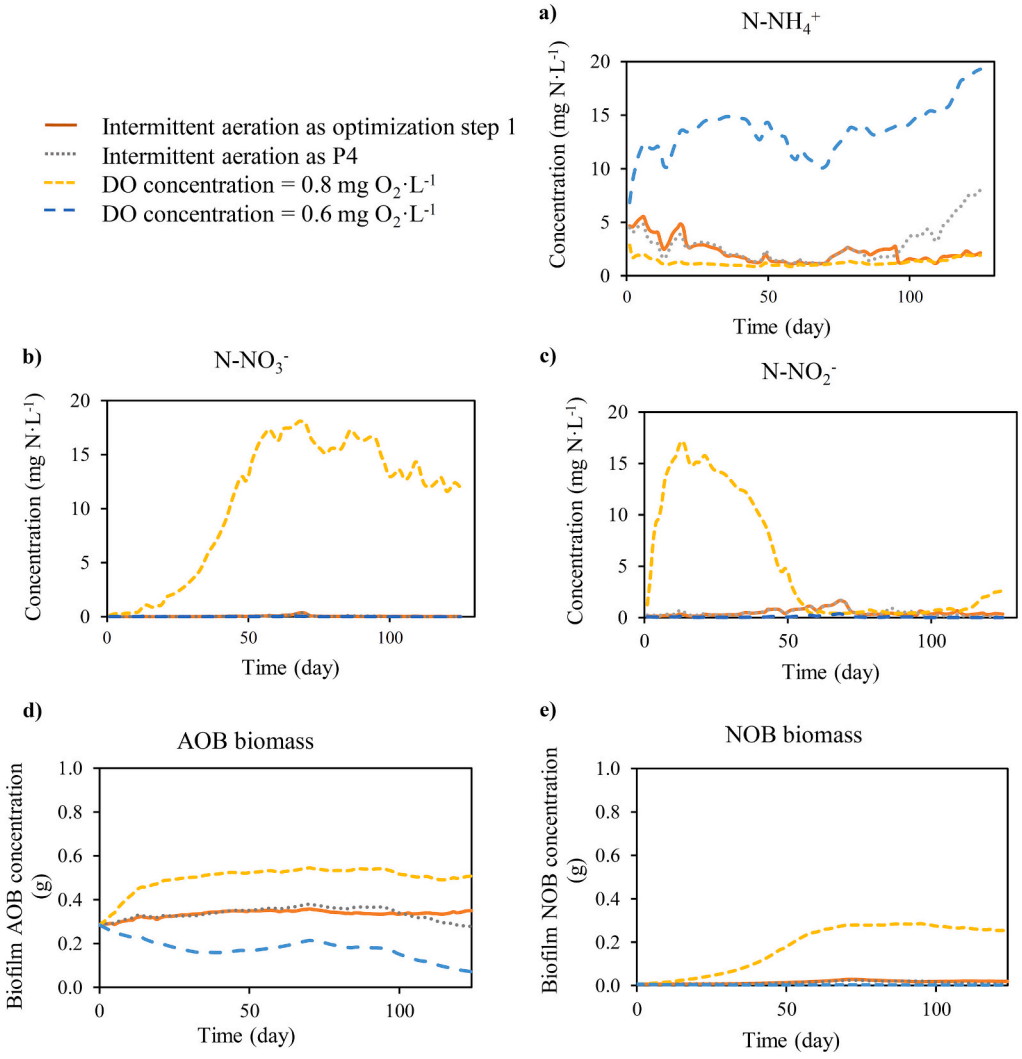

Fig. 4. Temporal profiles of the simulated concentrations of nitrogenous compounds, AOB, and NOB for the different aeration scenarios.

noted in N-NH_4^+ removal and AOB biomass concentration. In contrast, the abrupt growth of NOB biomass observed by modeling the experimental data, caused by the DO malfunction, produced an increase in N-NO_3^- concentration, which was completely absent in the simulated data.

The optimization scenarios presented in Table 4 and discussed below use the simulation in the absence of DO control failure as a reference for comparisons. The first step of optimization concerned the simulation of different aeration conditions, as reported in Table 4. Fig. 4 shows the profiles of N-NH_4^+, N-NO_3^-, and N-NO_2^- concentrations for all optimization scenarios. Specifically, a constant DO concentration of 0.6 mg $O_2 \cdot L^{-1}$ had a negative impact in terms of N-NH_4^+ removal, as it reduced AOB activity. Instead, a constant DO value of 0.8 mg $O_2 \cdot L^{-1}$ caused excessive growth of the NOB biomass, resulting in a breakthrough of NO_3^- and NO_2^- concentrations. By comparing the simulated data in Fig. 4, it is clear that the intermittent aeration conditions (without DO failure) represent the best strategy for the efficient removal of N-NH_4^+, N-NO_3^- and N-NO_2^- as it resulted in maximum effluent values below 5.5, 0.4 and 1.7 mg N•L^{-1}, respectively.

In a second optimization step, the effect of changing the pH from 9.0 to 6.5 was evaluated, as shown in Fig. 5. According to Rahimi et al. [50], pH values ranging from 7.5 to 8.5 benefit NO_2^- accumulation. Compared to the initial conditions, all proposed pH changes caused an increase in the N-NH_4^+ level in the reactor. In particular, the highest N-NH_4^+ increase was observed at pH 9.0 due to AOB inhibition [51], although this pH also resulted in the highest NOB inhibition [52]. On the other hand, the lowest simulated pH value of 6.5 did not improve N removal, as it led to a slight increase in N-NH_4^+ concentration. Comparing the results obtained for a pH of 8.4 and 8.1, a higher NOB inhibition was observed at pH of 8.4 with no significant changes in AOB biomass and N-NH_4^+ concentrations. Thus, based on these simulations, a pH value of 8.4 can be considered the best solution to obtain sufficient NOB inhibition and good N removal efficiency, with an average effluent N-NH_4^+, N-NO_3^- and N-NO_2^- concentrations of 2.6, 0.04 and 0.5 mg N•L^{-1}, respectively. Based on the results of the first experimental campaign regarding the benefits of HRT reduction from 2 to 1 d [21], the impact of a further HRT reduction from 1 to 0.5 d was simulated by increasing the influent flow rate (Fig. 6).

Fig. 6 shows that an HRT reduction to 0.75 and 0.5 d caused an inhibition of the nitrifying activity. An HRT of 0.5 d led to the maximum decrease in AOB biomass to a value of 0.01 g at the end of the simulation period. Compared to the results obtained at an HRT of 1 d, an HRT reduction to 0.9 d resulted in a higher NOB inhibition and average N-NH_4^+, N-NO_3^- and N-NO_2^- concentrations of 4.0, 0.02, and 0.07 mg·L^{-1}, respectively, indicating favorable conditions for the shortcut SND process.

4. Conclusions

Mathematical modeling successfully reproduced complete and shortcut SND processes in lab-scale MBBRs based on the results obtained

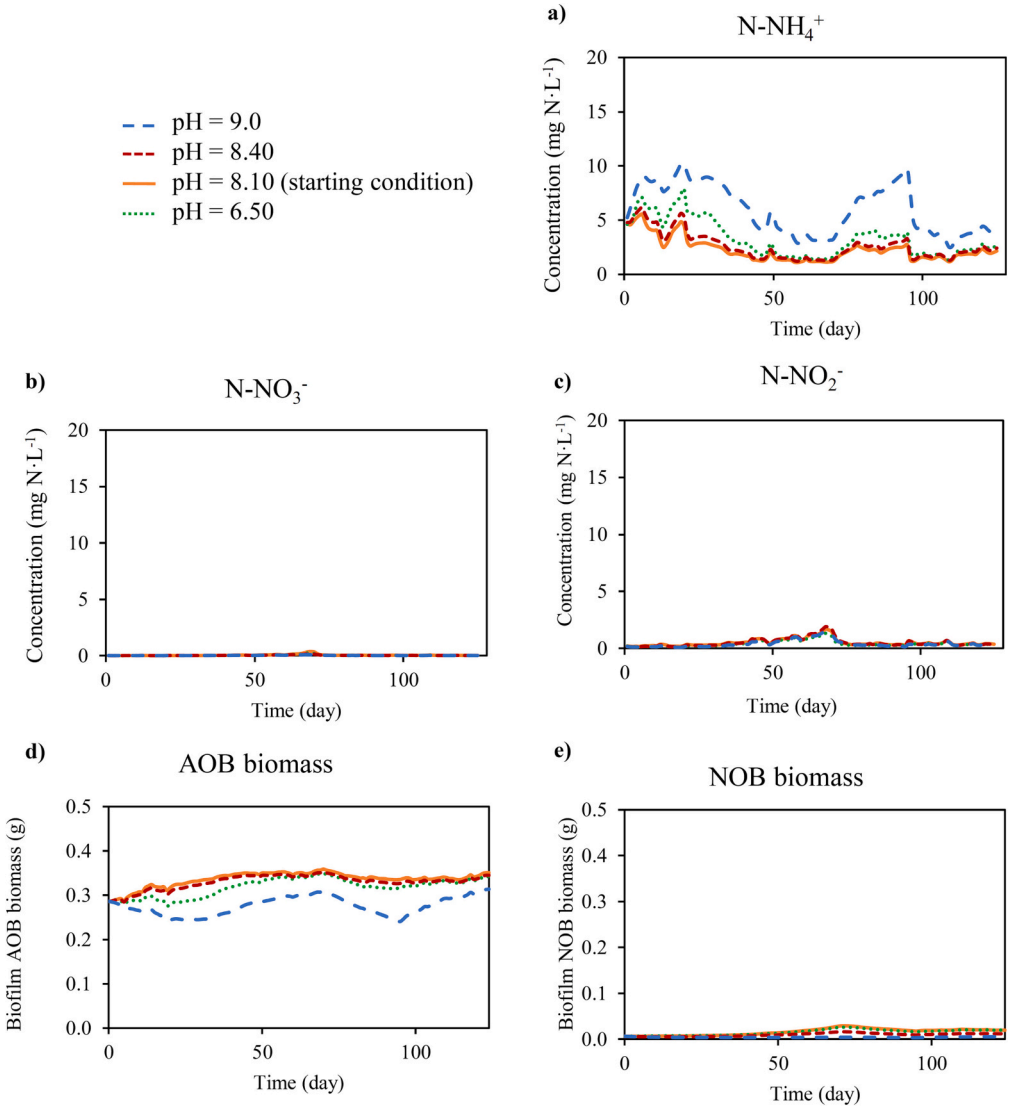

Fig. 5. Temporal profiles of the simulated concentrations of nitrogenous compounds, AOB, and NOB for different pH values.

from two different experimental campaigns. The sensitivity analysis was an effective tool to identify the most important parameters of the biofilm model. The calibrated and validated models showed a similar trend for soluble COD, $N\text{-}NH_4^+$, $N\text{-}NO_3^-$, $N\text{-}NO_2^-$, and $P\text{-}PO_4^{3-}$ concentrations compared to the experimental data. For all analyzed parameters, the *TIC* values ranged between 0.14 and 0.66 indicating a considerable model validity. Moreover, *NOF* values were almost constantly below 1 revealing an acceptable reproducibility between the experimental and modeled data. On the other hand, higher *TIC* and *NOF* values can be accepted due to the low absolute S_{ai} variance values. Process optimization via model simulation of different scenarios allowed to identify the best operating conditions to maximize N removal through the shortcut SND process. The results confirm that intermittent aeration can effectively induce and maintain NOB inhibition in the reactor with an average $N\text{-}NO_3^-$ concentration of 0.05 mg $N{\cdot}L^{-1}$. A pH value of 8.4 resulted in sufficient NOB inhibition and a low effluent $N\text{-}NH_4^+$ concentration of 2.57 mg $N{\cdot}L^{-1}$ (on average). An HRT of 0.9 d can be considered optimal as it resulted in average effluent $N\text{-}NH_4^+$, $N\text{-}NO_3^-$, and $N\text{-}NO_2^-$ concentrations of 4.0, 0.02, and 0.07 mg$\cdot L^{-1}$, respectively.

Funding

This work was supported by the PRIN 2022 project "BIOCORE" (cod. 2022J59S5Z), the Programma Operativo Nazionale (PON) FSE-FESR "Ricerca e Innovazione 2014-2020", Azione I.1 "Dottorati Innovativi con caratterizzazione industriale" and the Project "Energy efficiency of industrial products and processes", Research program "Piano Triennale della Ricerca del Sistema Elettrico Nazionale 2019–2021" funded by the Italian Ministry of Economic Development.

CRediT authorship contribution statement

Anna Lanzetta: Writing – review & editing, Writing – original draft, Visualization, Data curation. **Davide Mattioli:** Writing – review & editing, Writing – original draft, Visualization, Validation, Supervision, Software, Methodology, Investigation, Conceptualization. **Francesco Di Capua:** Writing – review & editing, Writing – original draft, Visualization, Validation, Supervision, Methodology, Investigation, Conceptualization. **Vincenzo Minieri:** Software, Investigation, Formal analysis, Data curation. **Stefano Papirio:** Writing – review & editing, Writing – original draft, Project administration, Funding acquisition. **Giovanni Esposito:** Writing – review & editing, Validation, Supervision, Project administration, Methodology, Investigation, Funding acquisition, Conceptualization.

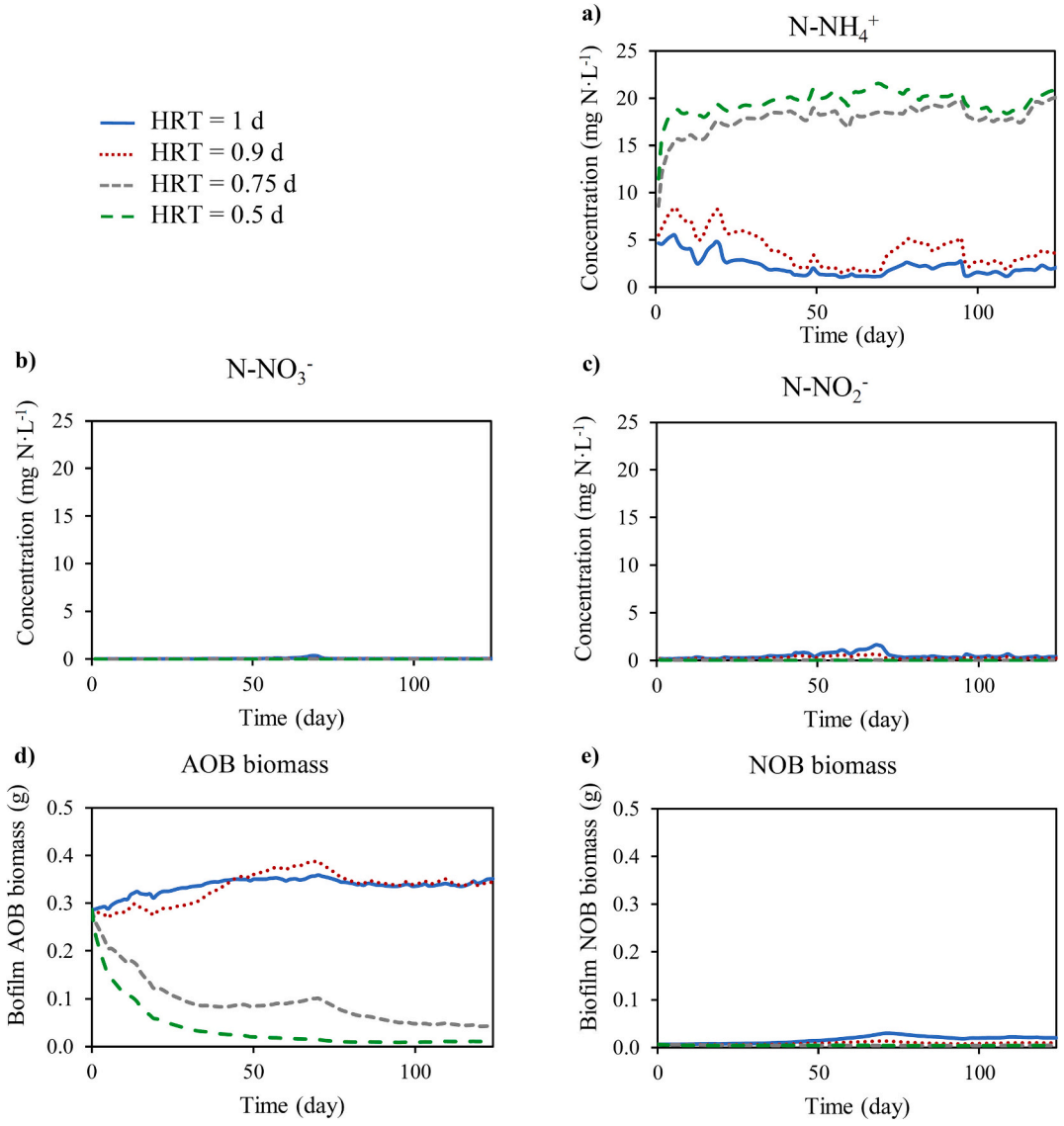

Fig. 6. Temporal profiles of the simulated concentrations of nitrogenous compounds, AOB, and NOB for different HRTs.

Declaration of competing interest

The authors declare that they have no known competing financial interests or personal relationships that could have appeared to influence the work reported in this paper.

Data availability

Data will be made available on request.

Appendix A. Supplementary data

Supplementary data to this article can be found online at https://doi.org/10.1016/j.jwpe.2024.105022.

References

[1] L. Chu, J. Wang, Nitrogen removal using biodegradable polymers as carbon source and biofilm carriers in a moving bed biofilm reactor, Chem. Eng. J. 170 (2011) 220–225, https://doi.org/10.1016/j.cej.2011.03.058.
[2] L.W. Ngatia, Y.P. Hsieh, D. Nemours, R. Fu, R.W. Taylor, Potential phosphorus eutrophication mitigation strategy: biochar carbon composition, thermal stability and pH influence phosphorus sorption, Chemosphere 180 (2017) 201–211, https://doi.org/10.1016/j.chemosphere.2017.04.012.
[3] G. Zou, S. Papirio, E.D. van Hullebusch, J.A. Puhakka, Fluidized-bed denitrification of mining water tolerates high nickel concentrations, Bioresour. Technol. 179 (2015) 284–290, https://doi.org/10.1016/j.biortech.2014.12.044.
[4] S. Papirio, G. Esposito, F. Pirozzi, Biological inverse fluidized-bed reactors for the treatment of low pH- and sulphate-containing wastewaters under different COD/SO2-4 conditions, Environ. Technol. (United Kingdom). 34 (2013) 1141–1149, https://doi.org/10.1080/09593330.2012.737864.
[5] P.L. Rittman, B.E. McCarty, Environmental Biotechnology:Principles and Applications, 2001.
[6] Metcalf & Eddy, Wastewater engineering: treatment, disposal, and reuse, 1991.
[7] M.K. Winkler, L. Straka, New directions in biological nitrogen removal and recovery from wastewater, Curr. Opin. Biotechnol. 57 (2019) 50–55, https://doi.org/10.1016/j.copbio.2018.12.007.
[8] L. Yan, S. Liu, Q. Liu, M. Zhang, Y. Liu, Y. Wen, Z. Chen, Y. Zhang, Q. Yang, Improved performance of simultaneous nitrification and denitrification via nitrite in an oxygen-limited SBR by alternating the DO, Bioresour. Technol. 275 (2019) 153–162, https://doi.org/10.1016/j.biortech.2018.12.054.
[9] X. Li, H. Nan, H. Jiang, H. Wang, C. Wang, Research trends on phosphorus removal from wastewater: a review and bibliometric analysis from 2000 to 2022, J. Water Process Eng. 55 (2023) 104201, https://doi.org/10.1016/j.jwpe.2023.104201.
[10] F. Di Capua, S. de Sario, A. Ferraro, A. Petrella, M. Race, F. Pirozzi, U. Fratino, D. Spasiano, Phosphorous removal and recovery from urban wastewater: current practices and new directions, Sci. Total Environ. 823 (2022) 153750, https://doi.org/10.1016/j.scitotenv.2022.153750.
[11] N. Di Costanzo, A. Cesaro, F. Di Capua, G. Esposito, Exploiting the nutrient potential of anaerobically digested sewage sludge: a review, Energies 14 (2021) 1–25, https://doi.org/10.3390/en14238149.

[12] R. Liu, X. Hao, Q. Chen, J. Li, Research advances of Tetrasphaera in enhanced biological phosphorus removal: a review, Water Res. 166 (2019), https://doi.org/10.1016/j.watres.2019.115003.
[13] J.T. Bunce, E. Ndam, I.D. Ofiteru, A. Moore, D.W. Graham, A review of phosphorus removal technologies and their applicability to small-scale domestic wastewater treatment systems, Front. Environ. Sci. 6 (2018) 1–15, https://doi.org/10.3389/fenvs.2018.00008.
[14] A.J. Schuler, D. Jenkins, Enhanced biological phosphorus removal from wastewater by biomass with different phosphorus contents, part II: anaerobic adenosine triphosphate utilization and acetate uptake rates, Water Environ. Res. 75 (2003) 499–511, https://doi.org/10.2175/106143003x141295.
[15] F. Di Capua, F. Iannacone, F. Sabba, G. Esposito, Simultaneous nitrification–denitrification in biofilm systems for wastewater treatment: key factors, potential routes, and engineered applications, Bioresour. Technol. 361 (2022) 127702, https://doi.org/10.1016/j.biortech.2022.127702.
[16] W. Ma, Y. Han, W. Ma, H. Han, H. Zhu, C. Xu, K. Li, D. Wang, Enhanced nitrogen removal from coal gasification wastewater by simultaneous nitrification and denitrification (SND) in an oxygen-limited aeration sequencing batch biofilm reactor, Bioresour. Technol. 244 (2017) 84–91, https://doi.org/10.1016/j.biortech.2017.07.083.
[17] M. Zaman, M. Kim, G. Nakhla, Simultaneous nitrification-denitrifying phosphorus removal (SNDPR) at low DO for treating carbon-limited municipal wastewater, Sci. Total Environ. 760 (2021) 143387, https://doi.org/10.1016/j.scitotenv.2020.143387.
[18] R.J. Zeng, R. Lemaire, Z. Yuan, J. Keller, Simultaneous nitrification, denitrification, and phosphorus removal in a lab-scale sequencing batch reactor, Biotechnol. Bioeng. 84 (2003) 170–178, https://doi.org/10.1002/bit.10744.
[19] E.V. Münch, P. Lant, J. Keller, Simultaneous nitrification and denitrification in bench-scale sequencing batch reactors, Water Res. 30 (1996) 277–284, https://doi.org/10.1016/0043-1354(95)00174-3.
[20] R. Huang, T. Meng, G. Liu, S. Gao, J. Tian, Simultaneous nitrification and denitrification in membrane bioreactor: effect of dissolved oxygen, J. Environ. Manag. 323 (2022), https://doi.org/10.1016/j.jenvman.2022.116183.
[21] F. Iannacone, F. Di Capua, F. Granata, R. Gargano, F. Pirozzi, G. Esposito, Effect of carbon-to-nitrogen ratio on simultaneous nitrification denitrification and phosphorus removal in a microaerobic moving bed biofilm reactor, J. Environ. Manag. 250 (2019) 109518, https://doi.org/10.1016/j.jenvman.2019.109518.
[22] F. Iannacone, F. Di Capua, F. Granata, R. Gargano, G. Esposito, Simultaneous nitrification, denitrification and phosphorus removal in a continuous-flow moving bed biofilm reactor alternating microaerobic and aerobic conditions, Bioresour. Technol. 310 (2020) 123453, https://doi.org/10.1016/j.biortech.2020.123453.
[23] F. Iannacone, F. Di Capua, F. Granata, R. Gargano, G. Esposito, Shortcut nitrification-denitrification and biological phosphorus removal in acetate- and ethanol-fed moving bed biofilm reactors under microaerobic/aerobic conditions, Bioresour. Technol. 330 (2021), https://doi.org/10.1016/j.biortech.2021.124958.
[24] M. Layer, M.G. Villodres, A. Hernandez, E. Reynaert, E. Morgenroth, N. Derlon, Limited simultaneous nitrification-denitrification (SND) in aerobic granular sludge systems treating municipal wastewater: mechanisms and practical implications, Water Res. X. 7 (2020) 100048, https://doi.org/10.1016/j.wroa.2020.100048.
[25] A. Lanzetta, F. Di Capua, B. Panneerselvam, D. Mattioli, G. Esposito, S. Papirio, Impact of Influent Composition and Operating Conditions on Carbon and Nitrogen Removal from Urban Wastewater in a Blanket Reactor, Energies 16 (2023) 6303, https://doi.org/10.3390/en16176303.
[26] A. Maurya, R. Kumar, A. Raj, Biofilm-based technology for industrial wastewater treatment: current technology, applications and future perspectives, World J. Microbiol. Biotechnol. 39 (2023), https://doi.org/10.1007/s11274-023-03567-7.
[27] M. Revilla, B. Galán, J.R. Viguri, An integrated mathematical model for chemical oxygen demand (COD) removal in moving bed biofilm reactors (MBBR) including predation and hydrolysis, Water Res. 98 (2016) 84–97, https://doi.org/10.1016/j.watres.2016.04.003.
[28] A.M. Faris, H.M. Zwain, M. Hosseinzadeh, H.S. Majdi, S.M. Siadatmousavi, Start-up and operation of novel EN-MBBR system for sidestreams treatment and sensitivity analysis modeling using GPS-X simulation, Alex. Eng. J. 61 (2022) 10805–10818, https://doi.org/10.1016/j.aej.2022.04.026.
[29] A. Eldyasti, G. Nakhla, J. Zhu, Development of a calibration protocol and identification of the most sensitive parameters for the particulate biofilm models used in biological wastewater treatment, Bioresour. Technol. 111 (2012) 111–121, https://doi.org/10.1016/j.biortech.2012.02.021.
[30] O. Wanner, P. Reichert, Mathematical modeling of mixed-culture biofilms, Biotechnol. Bioeng. 49 (1996) 172–184, https://doi.org/10.1002/(SICI)1097-0290(19960120)49:2<172::AID-BIT6>3.0.CO;2-N.
[31] M.R. Mattei, L. Frunzo, B. D'Acunto, Y. Pechaud, F. Pirozzi, G. Esposito, Continuum and discrete approach in modeling biofilm development and structure: a review, J. Math. Biol. 76 (2018) 945–1003, https://doi.org/10.1007/s00285-017-1165-y.
[32] EnviroSim Associates Ltd, Biowin 6 Help Manual, 2019.
[33] O. Wanner, W. Gujer, A multispecies biofilm model, Biotechnol. Bioeng. 28 (1986) 314–328.
[34] R. Ferrentino, A. Ferraro, M.R. Mattei, G. Esposito, G. Andreottola, Process performance optimization and mathematical modelling of a SBR-MBBR treatment at low oxygen concentration, Process Biochem. 75 (2018) 230–239, https://doi.org/10.1016/j.procbio.2018.08.023.
[35] A.A.L. Zinatizadeh, E. Ghaytooli, Simultaneous nitrogen and carbon removal from wastewater at different operating conditions in a moving bed biofilm reactor (MBBR): process modeling and optimization, J. Taiwan Inst. Chem. Eng. 53 (2015) 98–111, https://doi.org/10.1016/j.jtice.2015.02.034.
[36] L. Rieger, Guidelines for Using Activated Sludge Models (2012), https://doi.org/10.2166/9781780401164.
[37] Sabine Julien, Modélisation et estimation pour le contrôle d'un procédé boues activées éliminant l'azote des eaux résiduaires urbaines, 1997.
[38] N. Hvala, S. Strmčnik, D. Šel, S. Milanič, B. Banko, Influence of model validation on proper selection of process models - an industrial case study, Comput. Chem. Eng. 29 (2005) 1507–1522, https://doi.org/10.1016/j.compchemeng.2004.11.013.
[39] M. Zeng, A. Soric, N. Roche, Modeling partial nitrification and denitrification in a hybrid biofilm reactor: calibration by retention time distribution and respirometric tests, Environ. Sci. Pollut. Res. 22 (2015) 12849–12860, https://doi.org/10.1007/s11356-014-3667-0.
[40] A. Rajta, R. Bhatia, H. Setia, P. Pathania, Role of heterotrophic aerobic denitrifying bacteria in nitrate removal from wastewater, J. Appl. Microbiol. 128 (2020) 1261–1278, https://doi.org/10.1111/jam.14476.
[41] S. Ge, S. Wang, X. Yang, S. Qiu, B. Li, Y. Peng, Detection of nitrifiers and evaluation of partial nitrification for wastewater treatment: a review, Chemosphere 140 (2015) 85–98, https://doi.org/10.1016/j.chemosphere.2015.02.004.
[42] J. Guerrero, A. Guisasola, J.A. Baeza, The nature of the carbon source rules the competition between PAO and denitrifiers in systems for simultaneous biological nitrogen and phosphorus removal, Water Res. 45 (2011) 4793–4802, https://doi.org/10.1016/j.watres.2011.06.019.
[43] E. Casey, B. Glennon, G. Hamer, Biofilm development in a membrane-aerated biofilm reactor: effect of flow velocity on performance, Biotechnol. Bioeng. 67 (2000) 476–486, https://doi.org/10.1002/(SICI)1097-0290(20000220)67:4<476::AID-BIT11>3.0.CO;2-2.
[44] M.C.M. Van Loosdrecht, J.J. Heijnen, H. Eberl, J. Kreft, C. Picioreanu, Mathematical Modelling of Biofilm Structures, 2002.
[45] J.P. Boltz, E. Morgenroth, D. Brockmann, C. Bott, W.J. Gellner, P.A. Vanrelleghem, Critical Components of Biofilm Models for Engineering Practice to Cite this Version : HAL Id : Hal-01190424 Critical Components of Biofilm Models for Engineering, WWTmod2010 - 2nd IWA/WEF Wastewater Treat, Model, Semin, 2015.
[46] Z.R. Hu, M.C. Wentzel, G.A. Ekama, Modelling biological nutrient removal activated sludge systems - a review, Water Res. 37 (2003) 3430–3444, https://doi.org/10.1016/S0043-1354(03)00168-4.
[47] W. Trojanowicz, W. Styka, T. Baczynski, Experimental determination of kinetic parameters for heterotrophic microorganisms in bioflim under petrochemical wastewater conditions, Pol. J. Environ. Stud. 18 (2009) 913–921.
[48] M.C.M. Van L. Mogens Henze, W. Gujer, T. Mino, Activated Sludge Models ASM1, ASM2, ASM2d and ASM3, reprint,), IWA Publishing, London, 2000.
[49] C.M. López-Vázquez, C.M. Hooijmans, D. Brdjanovic, H.J. Gijzen, M.C.M. van Loosdrecht, Factors affecting the microbial populations at full-scale enhanced biological phosphorus removal (EBPR) wastewater treatment plants in the Netherlands, Water Res. 42 (2008) 2349–2360, https://doi.org/10.1016/j.watres.2008.01.001.
[50] S. Rahimi, O. Modin, I. Mijakovic, Technologies for biological removal and recovery of nitrogen from wastewater, Biotechnol. Adv. 43 (2020) 107570, https://doi.org/10.1016/j.biotechadv.2020.107570.
[51] E. Jiménez, J.B. Giménez, A. Seco, J. Ferrer, J. Serralta, Effect of pH, substrate and free nitrous acid concentrations on ammonium oxidation rate, Bioresour. Technol. 124 (2012) 478–484, https://doi.org/10.1016/j.biortech.2012.07.079.
[52] E. Jiménez, J.B. Giménez, M.V. Ruano, J. Ferrer, J. Serralta, Effect of pH and nitrite concentration on nitrite oxidation rate, Bioresour. Technol. 102 (2011) 8741–8747, https://doi.org/10.1016/j.biortech.2011.07.092.
[53] K.F. Liau, T. Shoji, Y.H. Ong, A.S.M. Chua, H.K. Yeoh, P.Y. Ho, Kinetic and stoichiometric characterization for efficient enhanced biological phosphorus removal (EBPR) process at high temperatures, Bioprocess Biosyst. Eng. 38 (2015) 729–737, https://doi.org/10.1007/s00449-014-1313-3.
[55] V. Van Huynh, M.T.T. Ngo, T. Itayama, M.B. Nguyen, T.D.H. Vo, T.K.Q. Vo, V. G. Le, S. Jie You, P.T. Nguyen, X.T. Bui, Dynamic of microbial community in simultaneous nitrification and denitrification process: a review, Bioresour. Technol. Reports. 22 (2023), https://doi.org/10.1016/j.biteb.2023.101415.
[57] K. Masmoudi Jabri, T. Fiedler, A. Saidi, E. Nolde, M. Ogurek, S.U. Geissen, L. Bousselmi, Steady-state modeling of the biodegradation performance of a multistage moving bed biofilm reactor (MBBR) used for on-site greywater treatment, Environ. Sci. Pollut. Res. 26 (2019) 19047–19062, https://doi.org/10.1007/s11356-018-3984-9.